

## Controlling Polymersome Size through Microfluidic-Assisted Self-Assembly: Enabling 'Ready to Use' formulations for biological applications

Martin, Anouk<sup>(a)</sup>, Lalanne, Pierre<sup>(a)</sup>, Weber-Vax, Amélie<sup>(a)</sup>, Mutschler, Angela<sup>(a)</sup>, Lecommandoux, Sébastien<sup>(a)</sup>

(a) *Université de Bordeaux, CNRS, Bordeaux INP, LCPO, UMR 5629, 33600 Pessac, France*

Corresponding author: [sebastien.lecommandoux@u-bordeaux.fr](mailto:sebastien.lecommandoux@u-bordeaux.fr)

### Abstract

The self-assembly of poly(ethylene glycol)-*block*-poly(trimethylene carbonate) PEG-*b*-PTMC copolymers into vesicles, also referred as polymersomes, was evaluated by solvent displacement using microfluidic systems. Two microfluidic chips with different flow regimes (micromixer and Herringbone) were used and the impact of process conditions on vesicle formation was evaluated. As polymersomes are sensitive to osmotic variations, their preparation under conditions allowing their direct use in biological medium is of major importance. We therefore developed a solvent exchange approach from DMSO (Dimethylsulfoxide) to aqueous media with an osmolarity of 300 mOsm.L<sup>-1</sup>, allowing their direct use for biological evaluation. We evidenced that the organic/aqueous solvent ratio does not impact vesicle size, but the total flow rate and copolymer concentration have been observed to influence the size of polymersomes. Finally, nanoparticles with diameters ranging from 76 nm to 224 nm were confirmed to be vesicles through the use of multi-angle light scattering in combination with cryo-TEM (Cryo-Transmission Electron Microscopy) characterization.

**Keywords:** Microfluidic, polymersomes, size control, self-assembly, nanomedicine

### 1. Introduction

The scientific interest in the field of nanomedicine has continuously grown during the last decades, with a number of publications per year that has been multiplied more than 5 times between 2010 and 2021 [1]. Nanomedicine is defined by National Institute of Health (NIH) as a reference to highly specific medical intervention at the molecular level for curing disease or repairing damaged tissues, such as bone, muscle or nerve [2]. Consistent with this definition, numerous nanomaterials are currently under investigation in clinical trials or have already been approved by the Food and Drug Administration (FDA) for use in human health as imaging agents or medical treatments [3,4]. Systems that are designed may be as diverse as lipid-based vesicles (called liposomes), dendrimers, gold nanoparticles, quantum dots or carbon nanotubes, proven by the wide variety of nano-sized supramolecular systems being currently studied [5,6]. Among these, liposomes and polymeric carriers are two classes of nanomaterials at the forefront of the field [7]. As an example, the well-known Doxil<sup>®</sup>, a liposomal formulation encapsulating doxorubicin, was one of the first liposomal drug approved by the FDA in 1995 for the treatment of AIDS-related Kaposi's sarcoma[8]. Since then, many of lipid and polymeric nanoparticles have been approved and present on the pharmaceutical market [9,10].

Despite their early success and their specific ability to load both hydrophilic and hydrophobic drugs, liposomes are often described as nanocarriers with several drawbacks, including the non-controlled release of the encapsulated drug and their relative physical and chemical instability in biological environments [11,12]. This is why their polymer analogues, also referred as polymersomes, have attracted great interest. [13,14]. Discher and Eisenberg were the first to define polymersomes as "microscopic sacs" that enclose a volume whose membrane results from the self-assembly of amphiphilic copolymers into bilayer membrane [15]. Due to their thicker membrane and their ability to adjust membrane properties based on the molar mass of selected block copolymers, polymersomes are generally more stable than liposomes in biological media [16]. This also allows for better control of drug release compared to lipid nanocarriers [17]. Their hollow structure remains one of their strengths, providing the opportunity to load hydrophobic drugs in their membrane and hydrophilic drugs in the aqueous lumen [18,19]. Despite these benefits, this hollow structure is also one of their most important drawbacks, rendering them sensitive to osmotic pressure variations, similar to other

vesicular structures. Indeed, osmotic difference between the vesicle lumen and external phase can lead to hypertonic or hypotonic shock that consequently leads to vesicle deformation (into raspberry shape, bubbling or stomatocytes [20–24]) and eventually to leakage and disruption of the bilayer membrane [25,26], that can be developed advantageously if well-controlled. However, in drug-delivery systems, one of the main consequences is an early and non-controlled drug release profile. Polymersomes thus require controlled parameters during their formulation to be ready-to-use for *in vitro* / *in vivo* experiments in physiological relevant conditions.

Polymersomes result from the self-assembly of amphiphilic copolymers with a thermodynamically and kinetically controlled mechanism. The self-assembly process depends on several critical parameters, including the physicochemical properties of the block copolymer (e.g. global molar mass, hydrophilic to hydrophobic balance,...)[27], the appropriate selection of organic [28,29] and aqueous [30] solvent and the choice of the formulation technique. If film hydration or direct dissolution were the first approaches developed for liposomes, they have been followed by a multitude of other processes, including electroformation, nanoprecipitation, double emulsion, post-processing resizing (for instance by extrusion), some of these methods being recently implemented in microfluidics [31,32]. The choice of the process can significantly influence vesicle formation and size [33]. For instance, film hydration method preferably gives giant vesicles [34] (hydrodynamic diameter > 1  $\mu\text{m}$ ) and nanoprecipitation enables the formation of small to large vesicles (50 nm < diameter < 1  $\mu\text{m}$ ) [15]. Accurate control of vesicle size and dispersity is of great importance in nanomedicine to improve the biodistribution profile of vesicles, especially to optimize drug delivery profile and minimize potential side effects. Indeed, many (physico)chemical parameters influence the biodistribution profile of the nanocarrier (including renal excretion, liver capture or tissue targeting), in particular the molar mass and size of the nanocarrier [35,36]. For instance, the widely known enhance permeability retention (EPR) effect, a biological phenomenon that enhances the efficacy of cancer treatment through selective accumulation of the nanocarriers in the tumor environment, strongly depends on size, shape and surface properties of the selected colloidal system [37,38].

The use of a microfluidic system for the self-assembly of polymer-based nanoparticles by nanoprecipitation has proven to be an effective strategy for achieving better control over vesicles size and dispersity, while providing high reproducibility of the process[39]. In this study, we further investigated the microfluidic-assisted self-assembly of a promising biodegradable and biocompatible amphiphilic copolymer : poly(ethylene glycol)-*block*-poly(trimethylene carbonate) PEG-*b*-PTMC[40]. Indeed, such block copolymers based on polycarbonate derivatives have been demonstrated to be highly interesting for biomaterials design, due to their low toxicity, biodegradability and potential functionality [41–48]. Dimethylsulfoxide (DMSO) was chosen as residual organic solvent. According to ICH Q3C guidelines, DMSO is considered as an organic solvent of class 3, which represents those with a low potential for toxicity in pharmaceutical formulation. Phosphate-Buffer Saline (PBS) was chosen as aqueous solvent because of its high relevance for biological purpose. Our study highlighted key factors that must be controlled in order to produce vesicles in a suspension ready to use both *in vitro* and *in vivo*. The influence of the aqueous solvent, the influence of mixing strategies utilizing two distinct types of microfluidic devices (Micromixer and Herringbone) and the impact of flow rate and copolymer concentration have been studied in detail. Our contribution provides important guidelines for the future development of vesicle formulation for clinical translation.

## 2. Materials and methods

### 2.1 Materials

PEG<sub>22</sub>-*b*-PTMC<sub>51</sub> was synthesized according to a previously reported method [40] (PEG<sub>22</sub>-*b*-PTMC<sub>51</sub> :  $f_{\text{PEG}} = 16.1\%$ ,  $D = 1.04$ ,  $M_n = 6200\text{ g}\cdot\text{mol}^{-1}$ ). Phosphate-Buffer Saline (PBS) 10X

was purchased from Euromedex. 10x refers to the concentration of the solution that needs to be diluted 10 times. 10x solution is composed of  $\text{KH}_2\text{PO}_4$ : 10.6 mM,  $\text{Na}_2\text{HPO}_4$ ,  $2\text{H}_2\text{O}$ : 30.0 mM, NaCl: 1.54 M. Dimethylsulfoxide (DMSO), with a purity determined in HPLC superior to 99.7 %, was purchased from Sigma-Aldrich. Micromixer chip was obtained from Dolomite Microfluidics and Herringbone chip from Darwin Microfluidics.

## 2.2 Colloidal characterization

**Dynamic Light Scattering (DLS):** Hydrodynamic diameter ( $D_h$ ) and particle size dispersity (PDI) were measured at 20 °C (with a pre-equilibration time for 30 s), using a Malvern Zetasizer Nano ZS90, equipped with a solid state HeNe laser ( $\lambda = 633$  nm) at a scattering angle of 90 °. Values of viscosity and refractive index were corrected according to the ratio of DMSO / PBS used. Size values are presented as the average of the Peak 1 measurement in intensity of three independent samples.  $D_h$  and PDI were calculated from autocorrelation functions using cumulant method.

**Multi Angle Light Scattering (MALS):** Hydrodynamic radius ( $R_H$ ) and radius of gyration ( $R_G$ ) of nanoparticles were measured at 25 °C using an ALV/CGS3 system composed of an ALV-5000 goniometer with HeNe laser ( $\lambda = 633$  nm) and an ALV-5000/EPP multiple  $\tau$  digital correlator (initial sampling time of 125 ns). Static light scattering (SLS) was performed from 25 ° to 149 ° by steps of 2 ° and DLS on the same range, by steps of 6 °. Samples were diluted if necessary up to 500 times.

$R_G$  was determined using Berry second order model on SLS measurements and  $R_H$  using Stoke-Einstein model on DLS measurements. Calculations and methods are provided in the *Supporting Information*.

**Cryo-Transmission Electron Microscopy (Cryo-TEM):** images were recorded at the “Institut de minéralogie, de Physique des Matériaux et de Cosmochimie” (Paris), as previously reported[40]. Mean diameter were calculated from measuring diameter of 50 vesicles, using ImageJ software.

**Osmometer :** *Löser automatic TypM 10-25  $\mu\text{L}$*  osmometer was used to measure the osmolarity of the different solutions.

## 2.3 Microfluidic assisted self-assembly

PBS solution was prepared by dilution ten times from the commercial reference and controlled to reach a pH of 7.4 and an osmolarity of  $300 \pm 4$  mOsm.L<sup>-1</sup>. PBS solution and copolymer dissolved in DMSO solution (variable concentrations from 1 to 30 mg.mL<sup>-1</sup>) were respectively filtered with 0.22  $\mu\text{m}$  cellulose acetate and 0.45  $\mu\text{m}$  PTFE membrane. As previously described [40], the Dolomite Microfluidics system was used with the micromixers chip. It was constituted of two pressure pumps (3200175), two flow rate sensors (3200097) and a micromixer chip (3200401) all connected with FEP tubing (1/16” $\times$  0.25 mm, 3200063). Under nitrogen pressure, flow rates were controlled by the Mitos Flow Control Center 2.5.17 software. One pump was filled with the filtered copolymer solution in DMSO and connected to the chip. The other pump was filled with filtered PBS. A camera was used to ensure the chip was dust free and air bubble free. DMSO flow rate was set according to calibration curve made on DMSO to overcome flow deviation due to DMSO viscosity. Herringbone chip was used with a syringe driver (Harvard Apparatus 33 Syringe Pump Dual Infuse) able to control two separate flow rates. A scheme of the setup and of the different microfluidic chips are represented on Figure 1. Flow rates were set according to experiment (from 20 to 800  $\mu\text{L}\cdot\text{min}^{-1}$ ). Organic solvent was then removed by dialysis against PBS using a 25 kDa cutoff dialysis membrane (Spectra/por<sup>®</sup>, 3 bath changes of 2 L each). All suspensions were prepared at room temperature.

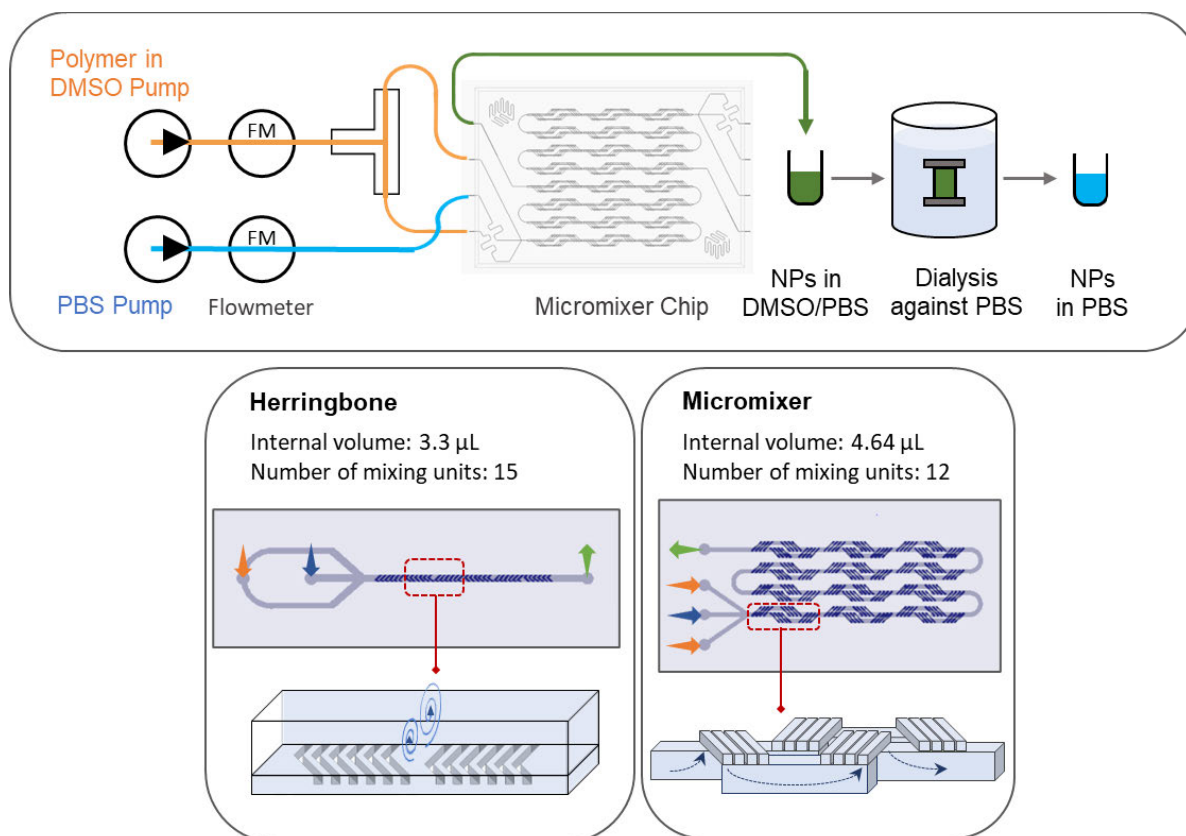


**Figure 1.** Schematic representation of microfluidic-assisted formulation of polymersomes followed by an overview of the microfluidic chips used for their preparation (Herringbone and micromixer).

#### 2.4. Osmotic pressure resistance test

Polymersome suspensions were obtained by microfluidic-assisted self-assembly using the micromixer chip. Filtered 10  $\text{mg}\cdot\text{mL}^{-1}$  copolymer solution in DMSO and filtered ultrapure water were used for the formulation of polymersomes and the organic solvent was removed by dialysis against ultrapure water. Ultrafiltration was then used to replace water by PBS with an osmolarity of 300  $\text{mOsm}\cdot\text{L}^{-1}$ . Three ultrafiltration cycles from 10 to 2 mL allow to obtain polymersomes in PBS, with an osmolarity of 281  $\text{mOsm}\cdot\text{L}^{-1}$ . Nano-objects in water and in PBS were then characterized by cryo-TEM to observe any effect of osmotic pressure on their size and shape.

#### 2.5. Critical Water Content (CWC) assays

We define the Critical Water Content (CWC) as the minimum of water required to be added in an organic solution containing the block copolymer to achieve the formation of self-assembled structure during a solvent-displacement process. For that purpose, intensity scattered by the solution was measured *in situ* by mobile DLS Vasco Kin<sup>TM</sup> (Cordouan), with a high stability laser source ( $\lambda = 638$  nm) used at 70 % of its power. In a typical experiment, the scattered signal of 1 mL of copolymer in DMSO solution (concentrated from 1 to 10  $\text{mg}\cdot\text{mL}^{-1}$ ) was observed while adding PBS. PBS was added at 40  $\mu\text{L}\cdot\text{mL}^{-1}$  with a syringe driver (Harvard Apparatus PHD 2000 Infusion), while solution was stirred at 250 rpm. This speed allows to homogenize the solution while positioning the laser between the magnetic stirrer and the meniscus. The influence of PBS flow rate was evaluated on CWC from 20 to 160  $\mu\text{L}\cdot\text{min}^{-1}$  (See *Supporting Information* Figure S1). The proposed home-made setup is illustrated in Figure 2A. The inflection point of the scattering curve was identified as the CWC, as it corresponds to the minimum amount of water required to trigger self-assembly of the block copolymer into nano-objects. Before the inflection point, free chains in solution cannot induce scattering signal while when polymer chains start to self-assemble, an increase in scattered light is detectable by the scattering instrument.[29,49] The scattered intensity was recorded and then treated on Origin85 software with [DOI: 10.1016/j.ijpharm.2023.123157](https://doi.org/10.1016/j.ijpharm.2023.123157)

the Savitzky-Golay smoothed function (Window 200 pts, Polynomial order 2). This smoothing is intended to withdraw noisy aspect of the curve due to experiment set up (light pollution, dust in the air, etc). Effect of smoothing is visible on Figure 2B.

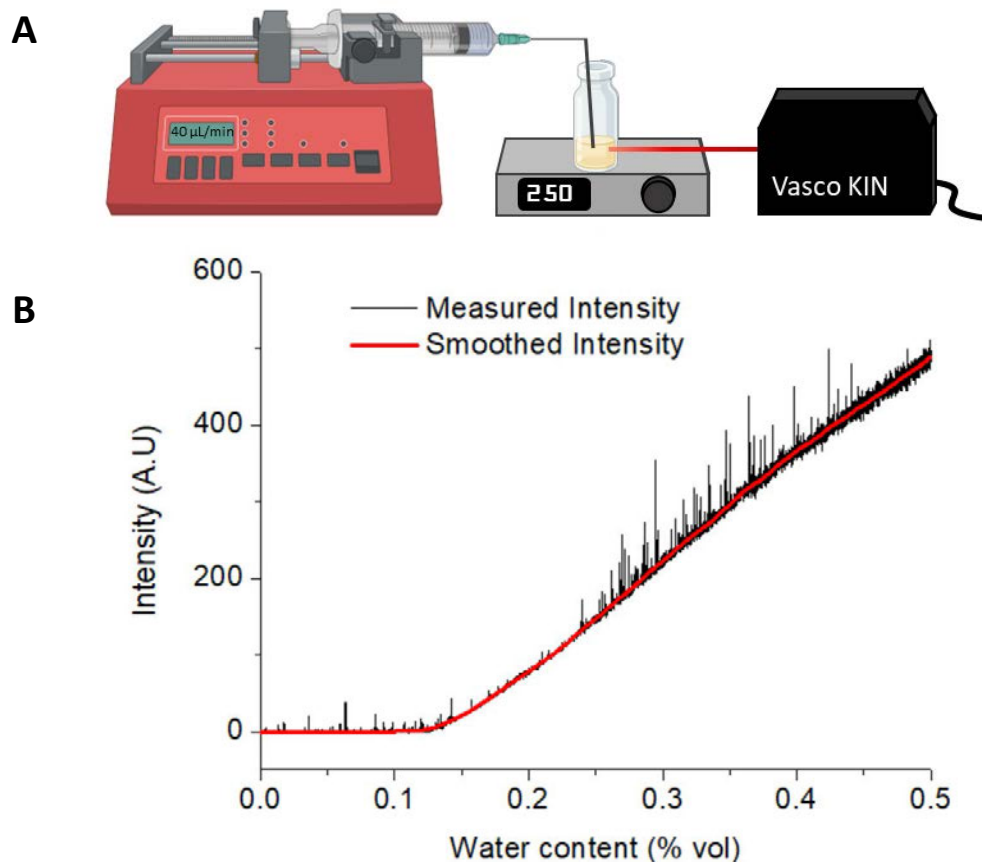


**Figure 2.** A) Schematic representation of “home-made” mobile DLS set-up. B) Scattered light intensity measured during the copolymer self-assembly, when aqueous solvent is added to copolymer dissolved in the organic solvent (initial copolymer concentration at  $2.5 \text{ mg}\cdot\text{mL}^{-1}$ ). Smoothing of the data given by Savitzky-Golay method.

### 3. Results and discussions

Controlling the osmotic pressure on polymersome is a crucial factor, from their formulation to *in vitro/in vivo* assays. To demonstrate this impact on our PEG-*b*-PTMC system, polymersomes were made first in a microfluidic-assisted self-assembly process using micromixer chip in pure water and separated into two batches. The first batch was kept in water while for the second batch, water was replaced during ultrafiltration by phosphate-buffered saline solution (PBS) with an osmotic pressure closed to  $300 \text{ mOsm}\cdot\text{L}^{-1}$ , corresponding to normal physiological conditions. According to cryo-TEM measurements, a difference is noticed before and after the change of external medium, where an overall change in vesicle diameter is monitored (Figure 3 A and B). The average diameter was measured from 67 to 34 nm, before and after replacement of water by saline buffer. This shrinking effect must be the result of a hypertonic shock that causes elongation and split of vesicles, as previously reported [21,50]. If we consider the use of vesicles for drug loading, a shape and size transformation may induce leakage and an uncontrolled burst release of the encapsulated drug. These results demonstrate that attention to the aqueous solvent during formulation is important when colloidal systems (such as vesicles) are intended to be used in a biological environment. For this reason, we decided to produce vesicles directly in PBS as aqueous solvent (with an osmolarity of  $300 \text{ mOsm}\cdot\text{L}^{-1}$ ) to prevent any possible premature drug leakage or colloidal destabilization during *in vitro / in vivo* assays.



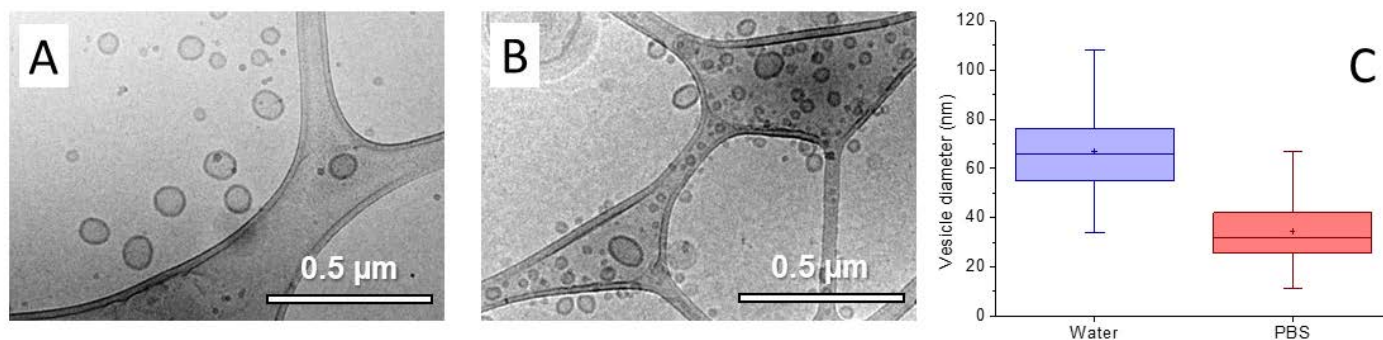


**Figure 3.** A) Cryo-TEM image of vesicles obtained in water. B) Cryo-TEM image of vesicles obtained in water and transferred in a  $\sim 300 \text{ mOsm.L}^{-1}$  phosphate-buffered saline (PBS) solution. Scale bar corresponds to  $0.5 \mu\text{m}$ . C) Box chart showing repartition of vesicles diameter before and after osmotic shock in PBS solution. Box chart shows maximum and minimum size (extremities), 25 and 75 percentiles (box), mean (cross) and median (line in the box). Each value corresponds to the mean size value of 150 vesicles and error bars correspond to standard deviations.

In order to find the relevant parameters to form stable nano-objects, we first determined the critical amount of water solution needed to induce copolymer self-assembly, defined as the critical water content (CWC). The amphiphilic block copolymer was dissolved in an organic solvent (DMSO) and PBS was added continuously with a low flow rate. The CWC was measured for several concentrations of polymer in DMSO, from 1 to  $10 \text{ mg.mL}^{-1}$ . A characteristic example of the experimental set-up and the scattered light intensity performed at a concentration of  $2.5 \text{ mg.mL}^{-1}$  is represented in Figure 2B. Figure 4 shows scattered light intensity for all evaluated copolymer concentrations. A reduction of the CWC with increasing copolymer concentration was observed, from 12.5 % v/v CWC for  $1 \text{ mg.mL}^{-1}$  of copolymer to 10.5 % v/v for  $10 \text{ mg.mL}^{-1}$ , in agreement with previous reports [49]. After demonstrating that the PEG-*b*-PTMC copolymer self-assembly capacity only occurs at a minimum aqueous solvent amount of approximately 10-12.5 % v/v, the aqueous solvent concentration was set far above the CWC threshold. Indeed, by maintaining a minimum of aqueous solvent of 50 % v/v, we ensure a stable self-assembly that will not be disrupted by post-formulation processes, such as dialysis purification.

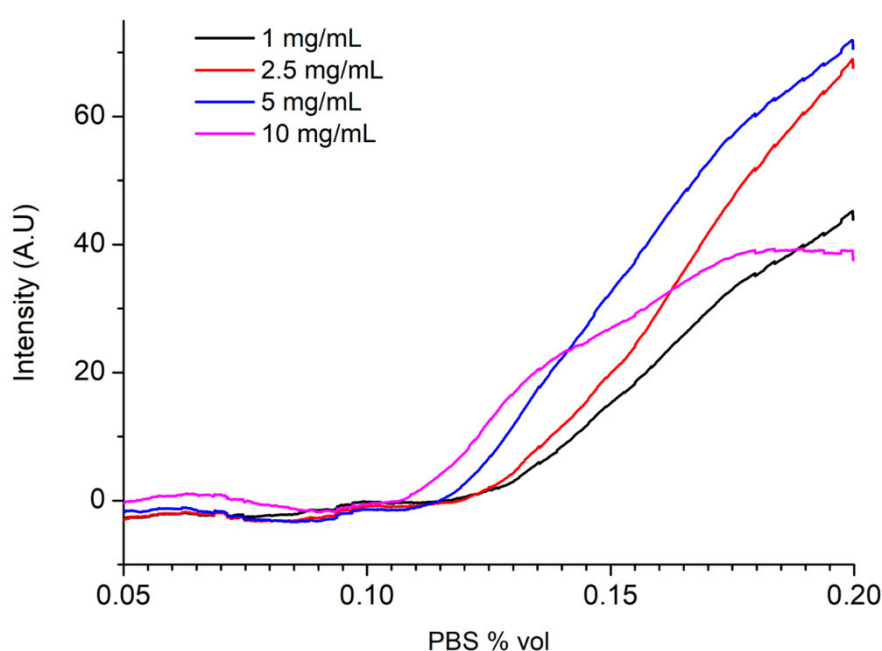


**Figure 4** : Scattered light intensity as measured by DLS during copolymer self-assembly when PBS is added to a polymer solution dissolved in DMSO and for a copolymer concentration ranging from 1 to 10 mg.mL<sup>-1</sup>. Represented curves are the average result of experiments carried out in triplicate and are smoothed by Savitzky-Golay method.

Nanoprecipitation was mainly carried out by manually adding organic phase to in a large excess of aqueous phase. However, the manual nanoprecipitation process is often limited by poor reproducibility and repeatability, leading to the formation of nanoparticles with a relatively high polydispersity index (PDI > 0.2). The implementation of processes allowing a better control of the mixing and the solvent flow allowed to solve the problem of the homogeneity of the nanoparticles. Specifically, microfluidic systems enable automated formulation of nanoparticles with high reproducibility and also offer the ability to continuously produce larger volumes of suspension for scale-up purposes. However, in typical microfluidic system, the flow is highly organized due to the small size of the channels. This results in mixing occurring primarily through diffusion, a slow process that leads to a low mixing speed, represented by classical chips with a ratio length / diameter of the channel that are very high. To overcome this limitation, various types of microfluidic mixers have been developed with three main strategies to increase the mixing speed [51]: (1) using multilaminar mixers (or micromixers) that create a subdivision of the initial flow into multiple sub-flows, reducing the width of the laminar flow phases and decreasing diffusion distances; (2) introducing transversal flow elements that create partially chaotic mixing, as seen in the case of herringbone mixers; and (3) causing flow collisions, resulting in smaller fluid segments and, in some cases, even turbulent mixing, as seen in impact-jet and vortex mixers.

The application of these mixers to the self-assembly of polymer nanoparticles by nanoprecipitation has resulted in effective particle size reduction and, in some cases, decrease polydispersity, with high reproducibility [39,52–54]. However, direct comparisons between these different mixers are limited, and to the best of our knowledge, rarely address the self-assembly polymer vesicles. We thus studied the impact of two microfluidic systems on the self-assembly of our PEG-*b*-PTMC block copolymer: the micromixer system, creating numerous flow subdivisions, and the Herringbone system, creating several chaotic flows. After varying the operating conditions (total flow rate, organic/aqueous solvent ratio, copolymer concentration), the evaluation of the size, the polydispersity index, and the structure of the obtained nanoparticles were analyzed.

Starting from a solution of 10 mg.mL<sup>-1</sup> of PEG-*b*-PTMC block copolymer in DMSO, the ratio of organic/aqueous solvent (DMSO/PBS) was adjusted from 50/50 to 20/80 (in % v/v). Total flow rate was kept at 1000  $\mu$ L.min<sup>-1</sup> for each ratio. All the samples obtained were purified of the organic solvent through a post-formulation process involving dialysis. Hydrodynamic diameter ( $D_H$ ) and PDI were systematically measured by DLS (Figure 5). As a result, the use of microfluidic assisted self-assembly enables the formation of nanoparticles with a hydrodynamic diameter around 100 nm and a PDI below 0.15, corresponding to the representation of a homogenous population of nanoparticles. When organic solvent fraction was increased from 20 to 50 % v/v, an increase of  $D_H$  was observed for both microfluidics systems (from 152 to 283 nm for micromixer chip and from 113 to 274 nm for Herringbone chip). It should be noted that the increase in the organic fraction is accompanied by an increase in the final concentration of copolymer in the suspension. For instance, when using 20 % organic solvent, the final copolymer concentration is 2 mg.mL<sup>-1</sup>, whereas using 50 % organic solvent results in a final copolymer concentration of 5 mg.mL<sup>-1</sup>. For a higher ratio of aqueous flow rate, shear stress between the streams increases, and the width of organic stream is decreased (lower concentration of block copolymer). This results in a formation of smaller nanoparticles and *vice versa*[51]. To study the influence of the solvent ratio, independently from the final copolymer concentration, same experiment was carried out by varying initial copolymer concentration to keep a final copolymer concentration of 2 mg.mL<sup>-1</sup>, using micromixer chip only. In this case, the size of the formed nanoparticles remains stable around 155 nm, highlighting that the final polymer concentration is the key parameter to tune the  $D_H$ . This phenomenon is consistent with a nucleation-growth mechanism and with experiments previously reported in literature [13].

In order to confirm the formation of vesicular structures, we decided to maintain a 20/80 (in % v/v) organic /aqueous ratio and compare the appearance of the obtained nanoparticles using the two microfluidic systems under these conditions. For both micromixer and Herringbone chips, samples were analyzed by MALS and Cryo-TEM. MALS results are shown in table I and Cryo-TEM acquisitions are available in Figure 6A. MALS enables the determination of the radius of gyration ( $R_G$ ) and the hydrodynamic radius ( $R_H$ ) of nanoparticles. A shape factor  $\rho=R_G/R_H$  can thus be estimated, with characteristic values of  $\rho=0.778$  for spherical micelles and  $\rho=1$  for polymersomes [55]. In our case, shape factors given by micromixer and Herringbone are between 1.07 and 1.22 (Table I), which are close enough to vesicular shape factor. Vesicles resulting from the self-assembly of the PEG-*b*-PTMC block copolymer can be obtained for both microfluidic systems, demonstrating that the type of fluid flow (subdivision or chaotic flow) has no impact on the structure of the obtained nanoparticles, but that a better control of these flows allow to obtain a homogeneous population of nanoparticles. Indeed, an efficient mixing between organic and aqueous solvent into microfluidic chip is the key parameter to control and the mixing time dictate the size and the distribution of nanoparticles. Usually, a short mixing time results in smaller particles with a lower PDI, as organic and aqueous solvents mix in a timeframe less than the time required for self-assembly to occur. In order to obtain a short mixing time, several parameters are important to control precisely and locally, such as the concentration of the copolymer, the ratio between organic and aqueous solvent and also the total flow rate. During manual nanoprecipitation, copolymer self-assembly takes place in an uncontrolled shear stress environment, which causes local concentration fluctuations resulting in larger particle sizes and a wider size distribution [51]

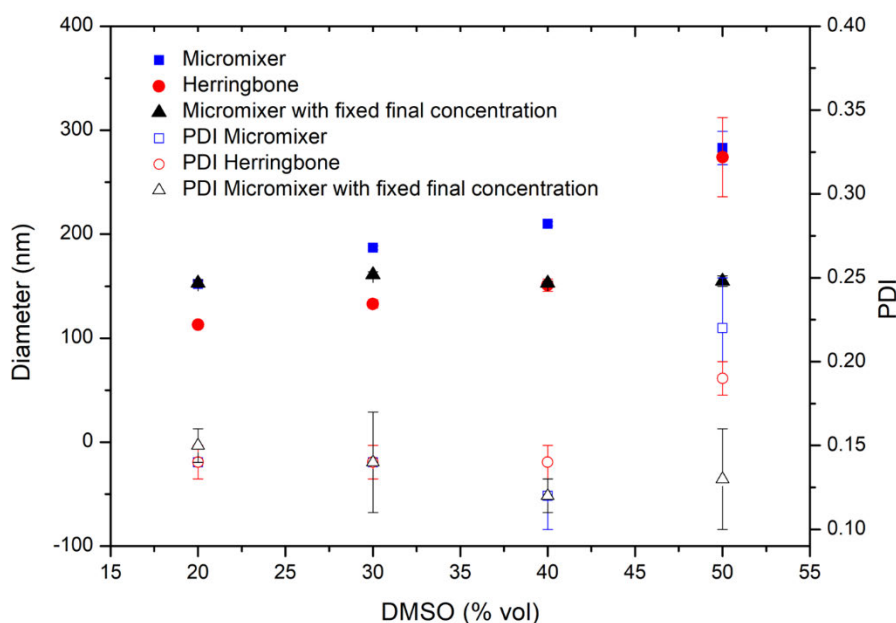


**Figure 5.** Evolution of hydrodynamic diameter (solid) and size dispersity PDI (open) of polymersomes, depending on aqueous/organic solvent ratio and microfluidic chip used. Each value corresponds to the mean size value of 3 experiments and error bars correspond to standard deviations.

We then decided to further investigate the concentration effect by using microfluidic assisted self-assembly with the micromixer chip, keeping 20/80 (% v/v) as the organic/aqueous ratio and total flow rate of  $1000 \mu\text{L}\cdot\text{min}^{-1}$ . We adjusted the concentration of copolymer in the final solution from  $0.2$  to  $6 \text{ mg}\cdot\text{mL}^{-1}$ . Organic solvent was removed by dialysis after microfluidic solvent displacement, and the solution was filtered with  $0.45 \mu\text{m}$  syringe filter cellulose acetate prior to DLS analysis. We observed an increase of diameter from  $76$  to  $224 \text{ nm}$  (Table 1) when final concentration was increased in the previously mentioned range. A linear trend can be observed between  $1$  and  $6 \text{ mg}\cdot\text{mL}^{-1}$ , following the equation :  $D_H = 3.37c \times 127.03$ , with  $D_H$  the hydrodynamic diameter measured by DLS (in nm), and



$c$  the initial copolymer concentration (in  $\text{mg}\cdot\text{mL}^{-1}$ ). The correlation coefficient for linear trend is  $R^2 = 0.9678$  (see *Supporting Information*, Figure S2). MALS was then performed to measure  $R_G$ ,  $R_H$  and deducing the shape factor  $\rho=R_G/R_H$  (Table I). SLS and DLS curves along with fitting equations are available in *Supporting Information*, Figure S4 – S13. The impact of the total flow rate on the hydrodynamic diameter was also investigated, as it can affect the diameter of the vesicles [56]. Microfluidic self-assembly formulation was performed, with a final concentration of copolymer at  $2 \text{ mg}\cdot\text{mL}^{-1}$  and with a variation of total flow rate of 100, 200, 500 and  $1000 \mu\text{L}\cdot\text{min}^{-1}$ . Diameter shows a tendency to increase when flow rate decreases, from 166 nm at  $1000 \mu\text{L}\cdot\text{min}^{-1}$ , to 218 nm at  $100 \mu\text{L}\cdot\text{min}^{-1}$  (Figure S3). This reduction facilitates a shorter mixing time, resulting in a decrease in nanoparticle size [51]. MALS confirm a vesicular shape formation with  $\rho = [1.10 ; 1.22]$ . Cryo-TEM also confirm the formation of bilayer membrane representative to polymersomes (Figure 6).

The observed increase in the diameter of polymersomes formulated in microfluidic system when the final copolymer concentration or when the total flow rate is increased, is consistent with a nucleation-growth mechanism, as previously proposed for this type of process [57,58]. Indeed, when the total flow rate decreases, interdiffusion of solvent occurs slower, delaying the freezing of structure due to a high amount of counter solvent for copolymer. Consequently, unimers self-assembly takes place for a longer time and nanoparticles with larger aggregation number and larger diameters are obtained. In addition, the increase in diameter upon increasing copolymer concentration may be the consequence of two phenomenon. First, a higher concentration of chain leads to a larger number of polymer chains available for self-assembly. Also, by increasing copolymer concentration, organic phase viscosity is increased, providing a higher mass transfer resistance. Interdiffusion of solvent is slowed down. Those two phenomena contribute to the formation of larger nanoparticles [31,45].

**Table I.** Hydrodynamic radius and radius of gyration of polymersomes (determined by DLS  $90^\circ$ , MALS and Cryo-TEM) obtained by microfluidic-assisted self-assembly with different mixing conditions. <sup>a</sup> Radius  $R_{\text{TEM}}$  is determined by an average measurement from approximately 50 vesicles.

Chip type	Concentration ( $\text{mg}\cdot\text{mL}^{-1}$ )	Total flow rate ( $\mu\text{L}\cdot\text{min}^{-1}$ )	DLS $90^\circ$		MALS			Cryo-TEM
			$R_H$ (nm)	PDI	$R_G$ (nm)	$R_H$ (nm)	$R_G/R_H$	$R_{\text{TEM}}^a$ (nm)
Herringbone	10	1000	57	0.14	58	52	1.07	$36 \pm 18$
Micromixer	10	1000	83	0.14	82	67	1.22	$72 \pm 16$
	10	500	85	0.11	90	76	1.19	
	10	200	104	0.13	75	68	1.10	
	10	100	109	0.13	90	77	1.17	
	1	1000	38	0.14	33	35	0.95	$49 \pm 9$
	5	1000	65	0.13	72	60	1.21	
	10	1000	83	0.14	82	67	1.22	
	15	1000	85	0.13	102	75	1.36	
	20	1000	96	0.14	101	76	1.30	
	25	1000	104	0.14	111	87	1.27	
30	1000	112	0.20	117	84	1.40	$101 \pm 18$	

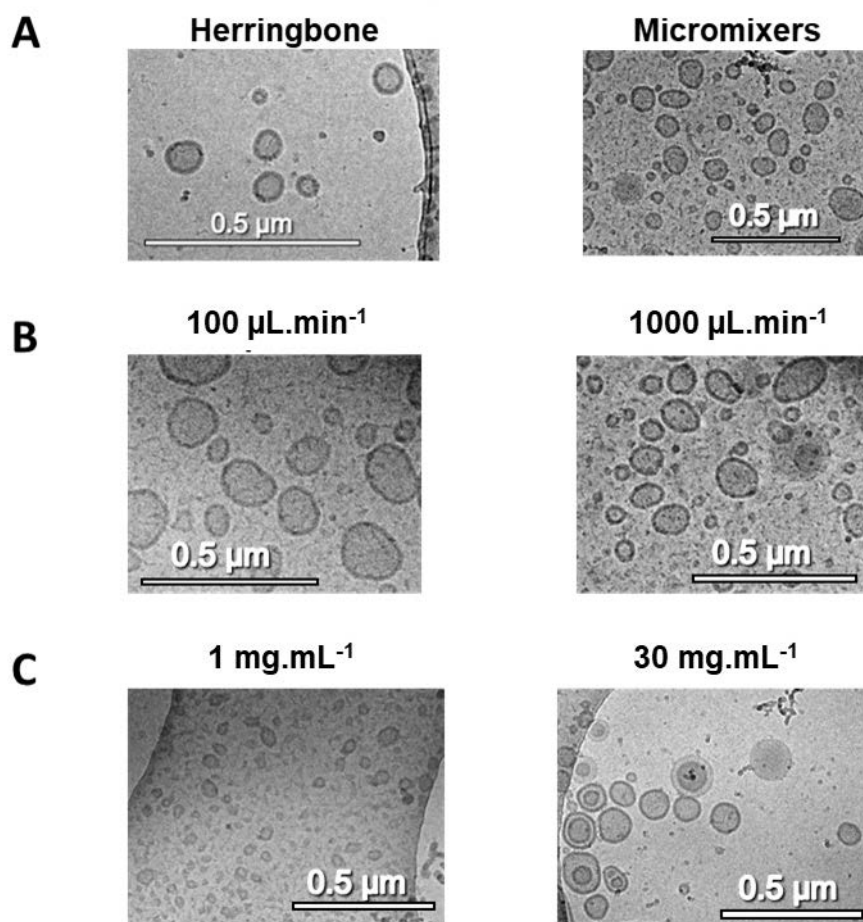


**Figure 6.** Representative TEM images for different conditions of polymersomes formulation. (A) when Herringbone and micromixer microfluidic systems are used. When using a micromixer system, the influence of processing conditions is investigated for two extreme total flow rates (100 and 1000  $\mu\text{L}\cdot\text{min}^{-1}$ ) (B) and also for two extreme PEG-*b*-PTMC concentrations (1 and 30  $\text{mg}\cdot\text{mL}^{-1}$ ) (C). Scale bar corresponds to 0.5  $\mu\text{m}$ .

#### 4. Conclusion

In this paper, we explored ways for generating polymeric vesicles, also called polymersomes, with tunable size, in conditions allowing them to be ready to use for *in vivo*/*in vitro* experiments. We first demonstrated the effect of transferring polymersomes made from pure water into a medium respecting physiological condition. The sensitivity of polymersomes to osmotic pressure variation has been demonstrated by a significant decrease in their size. In a drug delivery context, such transformation could obviously lead to an uncontrolled bursting effect if loaded vesicles are placed into biological fluids with osmolarity disparities. We have therefore succeeded in obtaining vesicles prepared in typical buffer close to physiological conditions ( $\text{pH} = 7.4$ ;  $300 \text{ mOsm}\cdot\text{L}^{-1}$ ) which will guarantee the integrity of the polymersomes when administrated. Critical water content (CWC) for copolymer self-assembly was measured around 11 % v/v and was used to optimize a minimal organic/water ratio to ensure the formation of stable vesicles during all the process of formulation (including self-assembly and purification step). In order to develop a method for formulating polymersomes that allows production with the highest reliability and reproducibility, two microfluidic chips with a fast-mixing process were compared. They showed similar behavior with respect to the aqueous/organic ratio, both forming vesicles under the conditions evaluated with a low value for the polydispersity index. Study on aqueous/organic ratio did not show effect on vesicle diameter. However, it highlighted the hypothetical effect of copolymer concentration on vesicle diameter. By

using micromixer chip, this parameter was further studied for a range of copolymer concentrations (0.2 to 6 mg.mL<sup>-1</sup> at final copolymer concentration), allowing us to reach colloidal system with diameters ranging from 76 to 224 nm. Concerning the impact of total flow rate on block copolymer self-assembly, our process conditions enhanced the effect on vesicle diameter growing from 160 nm for the highest flow rate (1000  $\mu$ L.min<sup>-1</sup>) to 218 nm for the lowest flow rate (100  $\mu$ L.min<sup>-1</sup>). In conclusion, in order to provide a highly reproducible process for vesicle formation in terms of size and polydispersity index, microfluidic-assisted self-assembly gives access to easily adjustable parameters to fine-tune their diameter. Vesicles with a diameter larger to 220 nm remains hard to reach with this method. However, as controlled self-assembly by microfluidic is dedicated to nanomedicine applications, we believe that size of nanoparticles should be in the range of 100 - 200 nm for suitable biodistribution profiles. Finally, the proposed microfluidic-assisted self-assembly approach for the production of reproducible, monodisperse and ready to use polymersomes for *in vivo/in vitro assays*, is a major advance in the production of nanocarriers, allowing for scale-up manufacturing while respecting pharmaceutical constraints.

## Acknowledgments

This work was sponsored by CNRS through a “80|Prime” PhD funding. The ANR TEPEE is also acknowledge for financial support, together with Université de Bordeaux and Bordeaux INP. The authors would also like to thank Jean-Michel Guinier from the Institut de minéralogie, de Physique des Matériaux et de Cosmochimie (Paris) for Cryo-TEM imaging, Christophe Schatz and Paul Marque for their support on MALS measurements. Jacques Leng (LOF UMR 5258 Bordeaux), Jean-Baptiste Salmon (LOF UMR 5258 Bordeaux) and Brice Calvignac (MINT UMR INSERM U1066 / UMR CNRS 6021 Angers) are also acknowledged for fruitful discussions related to microfluidics.

- [1] Timeline - Overview for nanomedicine in Publications - Dimensions n.d.  
[https://app.dimensions.ai/analytics/publication/overview/timeline?search\\_mode=content&search\\_text=nanomedicine&search\\_type=kws&search\\_field=full\\_search](https://app.dimensions.ai/analytics/publication/overview/timeline?search_mode=content&search_text=nanomedicine&search_type=kws&search_field=full_search) (accessed August 10, 2022).
- [2] Kantor LW. NIH Roadmap for Medical Research. *Alcohol Res Health* 2008;31:12–3.
- [3] Farjadian F, Ghasemi A, Gohari O, Roointan A, Karimi M, Hamblin MR. Nanopharmaceuticals and nanomedicines currently on the market: challenges and opportunities. *Nanomed* 2019;14:93–126. <https://doi.org/10.2217/nnm-2018-0120>.
- [4] Ventola CL. Progress in Nanomedicine: Approved and Investigational Nanodrugs. *Pharm Ther* 2017;42:742–55.
- [5] Kim BYS, Rutka JT, Chan WCW. Nanomedicine. *N Engl J Med* 2010;363:2434–43. <https://doi.org/10.1056/NEJMra0912273>.
- [6] Seleci M, Ag Seleci D, Bongartz R, Stahl F, Blume C, Scheper T. Smart multifunctional nanoparticles in nanomedicine. *BioNanoMaterials* 2016;17:33–41. <https://doi.org/10.1515/bnm-2015-0030>.
- [7] Zhang L, Gu FX, Chan JM, Wang AZ, Langer RS, Farokhzad OC. Nanoparticles in medicine: therapeutic applications and developments. *Clin Pharmacol Ther* 2008;83:761–9. <https://doi.org/10.1038/sj.clpt.6100400>.
- [8] Stewart S, Jablonowski H, Goebel FD, Arasteh K, Spittle M, Rios A, et al. Randomized comparative trial of pegylated liposomal doxorubicin versus bleomycin and vincristine in the treatment of AIDS-related Kaposi’s sarcoma. International Pegylated Liposomal Doxorubicin Study Group. *J Clin Oncol Off J Am Soc Clin Oncol* 1998;16:683–91. <https://doi.org/10.1200/JCO.1998.16.2.683>.
- [9] Duncan R. Polymer conjugates as anticancer nanomedicines. *Nat Rev Cancer* 2006;6:688–701. <https://doi.org/10.1038/nrc1958>.
- [10] Panzarini E, Inguscio V, Tenuzzo BA, Carata E, Dini L. Nanomaterials and autophagy: new insights in cancer treatment. *Cancers* 2013;5:296–319. <https://doi.org/10.3390/cancers5010296>.

- [11] Le Meins J-F, Schatz C, Lecommandoux S, Sandre O. Hybrid polymer/lipid vesicles: state of the art and future perspectives. *Mater Today* 2013;16:397–402. <https://doi.org/10.1016/j.mattod.2013.09.002>.
- [12] Che H, Hest JCM van. Stimuli-responsive polymersomes and nanoreactors. *J Mater Chem B* 2016;4:4632–47. <https://doi.org/10.1039/C6TB01163B>.
- [13] Leong J, Teo JY, Aakalu VK, Yang YY, Kong H. Engineering Polymersomes for Diagnostics and Therapy. *Adv Healthc Mater* 2018;7:e1701276. <https://doi.org/10.1002/adhm.201701276>.
- [14] LoPresti C, Lomas H, Massignani M, Smart T, Battaglia G. Polymersomes: nature inspired nanometer sized compartments. *J Mater Chem* 2009;19:3576–90. <https://doi.org/10.1039/B818869F>.
- [15] Discher DE, Eisenberg A. Polymer vesicles. *Science* 2002;297:967–73. <https://doi.org/10.1126/science.1074972>.
- [16] Rideau E, Dimova R, Schwille P, Wurm FR, Landfester K. Liposomes and polymersomes: a comparative review towards cell mimicking. *Chem Soc Rev* 2018;47:8572–610. <https://doi.org/10.1039/C8CS00162F>.
- [17] Matoori S, Leroux J-C. Twenty-five years of polymersomes: lost in translation? *Mater Horiz* 2020;7:1297–309. <https://doi.org/10.1039/C9MH01669D>.
- [18] Anajafi T, Mallik S. Polymersome-based drug-delivery strategies for cancer therapeutics. *Ther Deliv* 2015;6:521–34. <https://doi.org/10.4155/tde.14.125>.
- [19] Ahmed F, Pakunlu RI, Brannan A, Bates F, Minko T, Discher DE. Biodegradable polymersomes loaded with both paclitaxel and doxorubicin permeate and shrink tumors, inducing apoptosis in proportion to accumulated drug. *J Control Release Off J Control Release Soc* 2006;116:150–8. <https://doi.org/10.1016/j.jconrel.2006.07.012>.
- [20] Yanagisawa M, Imai M, Taniguchi T. Shape deformation of ternary vesicles coupled with phase separation. *Phys Rev Lett* 2008;100. <https://doi.org/10.1103/PhysRevLett.100.148102>.
- [21] Salva R, Le Meins J-F, Sandre O, Brûlet A, Schmutz M, Guenoun PP, et al. Polymersome Shape Transformation at the Nanoscale. *ACS Nano* 2013;7:9298–311. <https://doi.org/10.1021/nn4039589>.
- [22] Vanhille-Campos C, Šarić A. Modelling the dynamics of vesicle reshaping and scission under osmotic shocks. *Soft Matter* 2021;17:3798–806. <https://doi.org/10.1039/D0SM02012E>.
- [23] Carlsen A, Glaser N, Le Meins J-F, Lecommandoux S. Block Copolymer Vesicle Permeability Measured by Osmotic Swelling and Shrinking. *Langmuir* 2011;27:4884–90. <https://doi.org/10.1021/la105045m>.
- [24] Wilson D, Nolte R, Hest J. Autonomous movement of platinum-loaded stomatocytes. *Nat Chem* 2012;4:268–74. <https://doi.org/10.1038/nchem.1281>.
- [25] Peyret A, Ibarboure E, Tron A, Beauté L, Rust R, Sandre O, et al. Polymersome Popping by Light-Induced Osmotic Shock under Temporal, Spatial, and Spectral Control. *Angew Chem Int Ed Engl* 2017;56:1566–70. <https://doi.org/10.1002/anie.201609231>.
- [26] Larnaudie SC, Peyret A, Beaute L, Nassoy P, Lecommandoux SB. Photopolymerization-Induced Polymersome Rupture. *Langmuir ACS J Surf Colloids* 2019;35:8398–403. <https://doi.org/10.1021/acs.langmuir.9b01463>.
- [27] Mai Y, Eisenberg A. Self-assembly of block copolymers. *Chem Soc Rev* 2012;41:5969–85. <https://doi.org/10.1039/C2CS35115C>.
- [28] B. Pijpers IA, Meng F, Hest JCM van, A. Abdelmohsen LKE. Investigating the self-assembly and shape transformation of poly(ethylene glycol)-*b*-poly(*d*, *l*-lactide) (PEG-PDLLA) polymersomes by tailoring solvent-polymer interactions. *Polym Chem* 2020;11:275–80. <https://doi.org/10.1039/C9PY01089K>.
- [29] Yu Y, Zhang L, Eisenberg A. Morphogenic Effect of Solvent on Crew-Cut Aggregates of Amphiphilic Diblock Copolymers. *Macromolecules* 1998;31:1144–54. <https://doi.org/10.1021/ma971254g>.
- [30] Zhang L, Eisenberg A. Multiple Morphologies and Characteristics of “Crew-Cut” Micelle-like Aggregates of Polystyrene-*b*-poly(acrylic acid) Diblock Copolymers in Aqueous Solutions. *J Am Chem Soc* 1996;118:3168–81. <https://doi.org/10.1021/ja953709s>.

- [31] Bleul R, Thiermann R, Maskos M. Techniques To Control Polymersome Size. *Macromolecules* 2015;48:7396–409. <https://doi.org/10.1021/acs.macromol.5b01500>.
- [32] Liu Z, Zhou W, Qi C, Kong T. Interface Engineering in Multiphase Systems toward Synthetic Cells and Organelles: From Soft Matter Fundamentals to Biomedical Applications. *Adv Mater* 2020;32:2002932. <https://doi.org/10.1002/adma.202002932>.
- [33] Moghassemi S, Hadjizadeh A. Nano-niosomes as nanoscale drug delivery systems: an illustrated review. *J Control Release Off J Control Release Soc* 2014;185:22–36. <https://doi.org/10.1016/j.jconrel.2014.04.015>.
- [34] Sui X, Kujala P, Janssen G-J, Jong E de, Zuhorn IS, Hest JCM van. Robust formation of biodegradable polymersomes by direct hydration. *Polym Chem* 2015;6:691–6. <https://doi.org/10.1039/C4PY01288G>.
- [35] Alexis F, Pridgen E, Molnar LK, Farokhzad OC. Factors Affecting the Clearance and Biodistribution of Polymeric Nanoparticles. *Mol Pharm* 2008;5:505–15. <https://doi.org/10.1021/mp800051m>.
- [36] Owens DE, Peppas NA. Opsonization, biodistribution, and pharmacokinetics of polymeric nanoparticles. *Int J Pharm* 2006;307:93–102. <https://doi.org/10.1016/j.ijpharm.2005.10.010>.
- [37] Hobbs SK, Monsky WL, Yuan F, Roberts WG, Griffith L, Torchilin VP, et al. Regulation of transport pathways in tumor vessels: role of tumor type and microenvironment. *Proc Natl Acad Sci U S A* 1998;95:4607–12. <https://doi.org/10.1073/pnas.95.8.4607>.
- [38] Cabral H, Matsumoto Y, Mizuno K, Chen Q, Murakami M, Kimura M, et al. Accumulation of sub-100 nm polymeric micelles in poorly permeable tumours depends on size. *Nat Nanotechnol* 2011;6:815–23. <https://doi.org/10.1038/nnano.2011.166>.
- [39] Chen H, Celik AE, Mutschler A, Combes A, Runser A, Klymchenko AS, et al. Assembly of Fluorescent Polymer Nanoparticles Using Different Microfluidic Mixers. *Langmuir* 2022;38:7945–55. <https://doi.org/10.1021/acs.langmuir.2c00534>.
- [40] Lebleu C, Rodrigues L, Guigner J-M, Brûlet A, Garanger E, Lecommandoux S. Self-Assembly of PEG-b-PTMC Copolymers: Micelles and Polymersomes Size Control. *Langmuir* 2019;35:13364–74. <https://doi.org/10.1021/acs.langmuir.9b02264>.
- [41] WANG H, DONG JH, QIU\* AY, GU ZW. Studies on Properties and Drug Delivery Systems of PTMC-b-PEG-b-PTMC Block Copolymers. *J Macromol Sci Part A* 1998;35:811–20. <https://doi.org/10.1080/10601329808002013>.
- [42] Drappier C, Oliveira H, Sandre O, Ibarboure E, Combet S, Garanger E, et al. Self-assembled core-shell micelles from peptide- b -polymer molecular chimeras towards structure-activity relationships. *Faraday Discuss* 2013;166:83–100. <https://doi.org/10.1039/C3FD00098B>.
- [43] Ajiro H, Haramiishi Y, Chanthaset N, Akashi M. Polymer design using trimethylene carbonate with ethylene glycol units for biomedical applications. *Polym J* 2016;48:751–60. <https://doi.org/10.1038/pj.2016.35>.
- [44] Fukushima K. Poly(trimethylene carbonate)-based polymers engineered for biodegradable functional biomaterials. *Biomater Sci* 2015;4. <https://doi.org/10.1039/c5bm00123d>.
- [45] Sanson C, Schatz C, Le Meins J-F, Brûlet A, Soum A, Lecommandoux S. Biocompatible and Biodegradable Poly(trimethylene carbonate)-b-Poly(l-glutamic acid) Polymersomes: Size Control and Stability. *Langmuir* 2010;26:2751–60. <https://doi.org/10.1021/la902786t>.
- [46] Lebleu C. Polymersomes based on PEG-b-PTMC towards cell-mediated delivery of nanomedicines. phdthesis. Université de Bordeaux, 2019.
- [47] Ke X-Y, Lin Ng VW, Gao S-J, Tong YW, Hedrick JL, Yang YY. Co-delivery of thioridazine and doxorubicin using polymeric micelles for targeting both cancer cells and cancer stem cells. *Biomaterials* 2014;35:1096–108. <https://doi.org/10.1016/j.biomaterials.2013.10.049>.
- [48] Liu S, Ono RJ, Yang C, Gao S, Tan JYM, Hedrick JL, et al. Dual pH-Responsive Shell-Cleavable Polycarbonate Micellar Nanoparticles for in Vivo Anticancer Drug Delivery. *ACS AMI* 2018. <https://doi.org/10.1021/acsami.8b01954>.
- [49] Wang C-W, Sinton D, Moffitt MG. Morphological Control via Chemical and Shear Forces in Block Copolymer Self-Assembly in the Lab-on-Chip. *ACS Nano* 2013;7:1424–36. <https://doi.org/10.1021/nn305197m>.



- [50] Liu X, Stenhammar J, Wennerström H, Sparr E. Vesicles Balance Osmotic Stress with Bending Energy That Can Be Released to Form Daughter Vesicles. *J Phys Chem Lett* 2022;13:498–507. <https://doi.org/10.1021/acs.jpcllett.1c03369>.
- [51] Agha A, Waheed W, Stiharu I, Nerguizian V, Destgeer G, Abu-Nada E, et al. A review on microfluidic-assisted nanoparticle synthesis, and their applications using multiscale simulation methods. *Nanoscale Res Lett* 2023;18:18. <https://doi.org/10.1186/s11671-023-03792-x>.
- [52] Streck S, Neumann H, Nielsen H, Rades T, McDowell A. Comparison of bulk and microfluidics methods for the formulation of poly-lactic-co-glycolic acid (PLGA) nanoparticles modified with cell-penetrating peptides of different architectures. *Int J Pharm X* 2019;1:100030. <https://doi.org/10.1016/j.ijpx.2019.100030>.
- [53] Petit J, Polenz I, Baret J-C, Herminghaus S, Bäumchen O. Vesicles-on-a-chip: A universal microfluidic platform for the assembly of liposomes and polymersomes. *Eur Phys J E* 2016;39:59. <https://doi.org/10.1140/epje/i2016-16059-8>.
- [54] Thiele J, Steinhauser D, Pfohl T, Förster S. Preparation of Monodisperse Block Copolymer Vesicles via Flow Focusing in Microfluidics. *Langmuir* 2010;26:6860–3. <https://doi.org/10.1021/la904163v>.
- [55] Dautzenberg H. *Advances in polymer science*. Vol. 48. Light scattering from polymers. Hg. von H.-J. CANTOW u. a. ; Berlin/Heidelberg/New York: Springer-Verlag 1982, 167 S., Lwd., DM 98,—. *Acta Polym* 1984;35:433–433. <https://doi.org/10.1002/actp.1984.010350518>.
- [56] Thiermann R, Mueller W, Montesinos-Castellanos A, Metzke D, Löb P, Hessel V, et al. Size controlled polymersomes by continuous self-assembly in micromixers. *Polymer* 2012;53:2205–10. <https://doi.org/10.1016/j.polymer.2012.03.058>.
- [57] Shillcock JC. Spontaneous Vesicle Self-Assembly: A Mesoscopic View of Membrane Dynamics. *Langmuir* 2012;28:541–7. <https://doi.org/10.1021/la2033803>.
- [58] Uneyama T. Density functional simulation of spontaneous formation of vesicle in block copolymer solutions. *J Chem Phys* 2007;126:114902. <https://doi.org/10.1063/1.2463426>.

## Supporting Information for

### Microfluidic-assisted self-assembly of polymersomes: in vitro/vivo “ready to use” method with size control

Martin, Anouk <sup>(a)</sup>, Lalanne, Pierre<sup>(a)</sup>, Weber-Vax, Amélie<sup>(a)</sup>, Mutschler, Angela<sup>(a)</sup>, Lecommandoux, Sébastien <sup>(a)</sup>

(a) *Université de Bordeaux, CNRS, Bordeaux INP, LCPO, UMR 5629, 33600 Pessac, France*

## Table of content

1. General informations.....	1
1.1 Materials.....	1
1.2 Characterization techniques.....	1
2. Impact of water addition rate on Critical Water Content .....	2
3. Size variation depending on copolymer concentration .....	3
4. Size variation depending on total flow rate .....	3
5. Multi Angle Light Scattering analyzes.....	4
References.....	10

## 1. General informations

### 1.1 Materials

PEG<sub>22</sub>-*b*-PTMC<sub>51</sub> was synthesized according to a previously reported method[1]. Phosphate-Buffer Saline 10X (PBS) was purchased from Euromedex. Dimethylsulfoxide (DMSO) was purchased from Sigma-Aldrich (with a purity determined in HPLC superior to 99.7%). Micromixer chip was obtained from Dolomite Microfluidics and Herringbone chip from Darwin Microfluidics.

### 1.2 Characterization techniques

**Critical Water Content (CWC) measurement:** VASCO KIN<sup>TM</sup> from Courdouan Technologies was kindly loaned by the laboratory “Centre de Recherche Paul Pascal” (CRPP). VASCO KIN<sup>TM</sup> is a Diffusion Light Scattering (DLS) apparatus composed of a mobile head that proceed in a continuous measurement at 170 °, to obtain size distribution, scattered intensity or correlograms from analyzed solutions. Laser source is a high stability laser diode ( $\lambda = 638$  nm) which will be used at 70 % of its power. Measurements are controlled using NanoKin<sup>®</sup> software. Smoothing function of Origin85 software was used to withdraw noise from the signal. We used Savitzky-Golay smoothing function (Window 200 pts, Polynomial order 2).

**Dynamic Light Scattering (DLS):** Hydrodynamic diameter ( $D_h$ ) and particle size dispersity (PDI) were measured at 20 °C (pre-equilibration time for 30 s) using a Malvern Zetasizer Nano ZS90, equipped with a solid state HeNe laser ( $\lambda = 633$  nm) at a scattering angle of 90°. Values of viscosity and refractive index were corrected according to the mixture of organic/aqueous solvent (DMSO / PBS). Size values are presented as the average

of the Peak 1 measurement of three independent samples.  $D_h$  and PDI were calculated from autocorrelation functions using cumulant method.

**Multi Angle Light Scattering (MALS) measurement:** MALS measurements were performed using a ALV-5000 goniometer with a He-Ne laser ( $\lambda = 633 \text{ nm}$ ) and an ALV-5000/EPP multiple tau digital correlator. Solution to analyzed were placed in cylindrical quartz tubes and immersed in a filtered toluene bath maintained at  $25 \text{ }^\circ\text{C}$  correlator. Static light scattering (SLS) was performed from  $25^\circ$  to  $149^\circ$  by step of  $2^\circ$  and DLS on the same range of angle, by steps of  $6^\circ$ . Samples were diluted when needed, up to 500 times to obtain an almost constant attenuator all along measurement.  $R_G$  was determined using Berry second order model on SLS measurements and  $R_H$  using Stoke-Einstein model on DLS measurements. Data were normalized by signals for pure toluene and pure aqueous solvent. Using  $R_G$  and  $R_H$ , we can calculate shape factor  $\rho = R_G/R_H$ . This factor allows to know nature of the object depending on its value. If  $\rho = 1$ , objects are more likely to be vesicles,  $\rho=2$  is sign of cylindrical objects and if  $\rho=0.8$ , objects are more likely to be spheres or micelles.

## 2. Impact of water addition rate on Critical Water Content (CWC)

CWC is a key parameter to measure when studying copolymer self-assembly. This parameter represents water content needed to induce self-assembly from copolymer in organic solvent. It can be measured by following the light scattered by the copolymer solution when water is added. Indeed, free chains in an organic solvent do not scatter light instead of self-assembled objects. Thus, we can find the critical water content by measuring the signal of scattered light.

CWC is known to depend on the type of copolymer, solvent, and copolymer concentration. Light scattered by a solution of PEG-*b*-PTMC in DMSO at  $2.5 \text{ mg}\cdot\text{mL}^{-1}$  is first studied while adding water at 4 different speeds : 20, 40, 80 and  $160 \text{ }\mu\text{L}\cdot\text{mL}^{-1}$ . The observed results (Figure S1) confirm that slope break occurs at the same amount of PBS regardless of the flow rate.

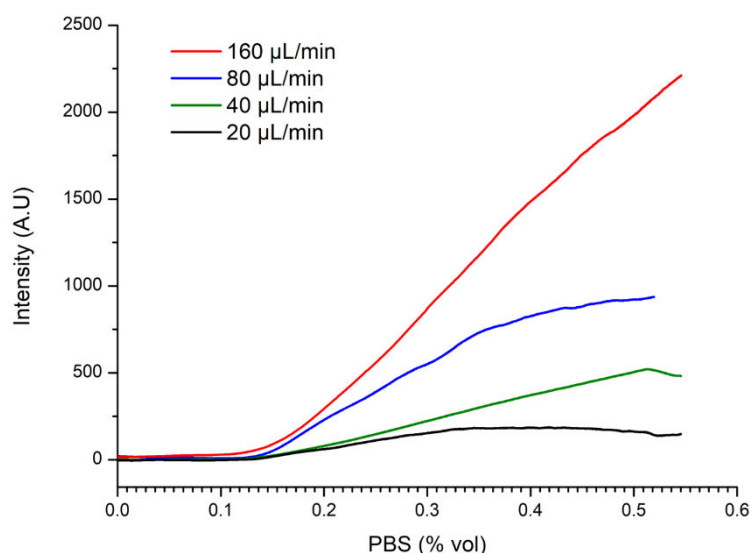


**Figure S1:** Scattered intensity from  $2.5 \text{ mg}\cdot\text{mL}^{-1}$  solution of copolymer in DMSO during PBS addition at different flow rates. Curves represent an average of signals from experiments done in triplicate.

### 3. Size variation depending on copolymer concentration

The variation of organic/aqueous solvent ratio without fixing final copolymer concentration showed that copolymer concentration influences the diameter of obtained vesicles, while no variation of diameter is observed with a fixed final concentration (Figure 5). By setting a ratio of DMSO/PBS of 20/80 (% v/v) and a total flow rate of  $1000 \mu\text{L}\cdot\text{min}^{-1}$ , initial copolymer concentration was varied from 1 to  $30 \text{ mg}\cdot\text{mL}^{-1}$  to proceed in microfluidic assisted self-assembly. Figure S2 illustrates results obtained from DLS  $90^\circ$  measurement on samples after dialysis.

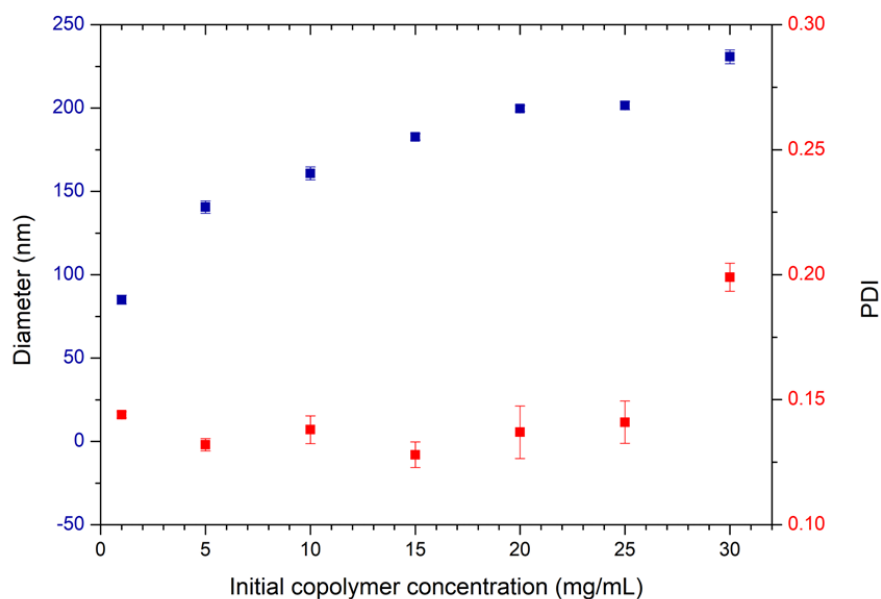


**Figure S2** : Diameter and PDI obtained by DLS  $90^\circ$  from microfluidic assisted self-assembly of  $\text{PEG}_{22}\text{-}b\text{-PTMC}_{51}$  samples starting with different copolymer concentrations. Linear regression is observed between 5 and  $30 \text{ mg}\cdot\text{mL}^{-1}$ , following the equation  $D_H = 3.37c \times 127.03$ , with  $D_H$  the hydrodynamic diameter (in nm), and  $c$  the initial copolymer concentration (in  $\text{mg}\cdot\text{mL}^{-1}$ ). The correlation coefficient is  $R^2 = 0.9678$ . Each value corresponds to the mean size value of 3 experiments and error bars correspond to standard deviations.

### 4. Size variation depending on total flow rate

Vesicle diameter is reported to be sensitive to mixing rate, relied to total flow rate in the case of microfluidic system [2]. We varied total flow rate from 100 to  $1000 \mu\text{L}\cdot\text{min}^{-1}$ , using Mitos Pressure Pumps, and a minimum total flow rate of  $50 \mu\text{L}\cdot\text{min}^{-1}$  is reached, using a Harvard Apparatus syringe driver, keeping an organic/aqueous ratio of 20/80 %vol and an initial copolymer concentration of  $10 \text{ mg}\cdot\text{mL}^{-1}$ . Figure S3 shows results obtained from DLS  $90^\circ$  measurement of samples after removing organic solvent by dialysis.

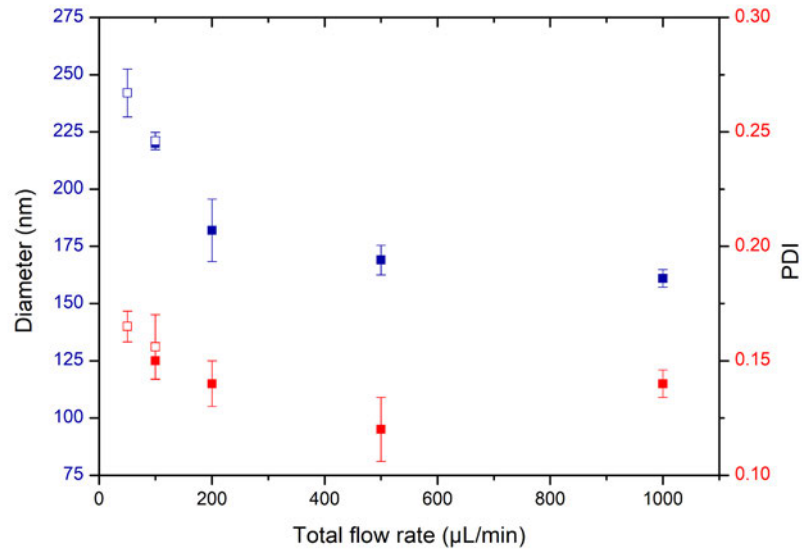


**Figure S3** : Diameter and PDI obtained by DLS 90° from microfluidic assisted self-assembly of PEG<sub>22</sub>-*b*-PTMC<sub>51</sub> samples starting with different total flow rates. Full squares samples are obtained using Mitos Pressure Pumps, but as they cannot reach low flow rate, Harvard Apparatus syringe driver were used to obtain samples represented by empty squares.

## 5. Multi Angle Light Scattering (MALS)

MALS was used to ensure vesicular shape of object made with microfluidic assisted self-assembly of PEG-*b*-PTMC. SLS and DLS measurement were performed as described above and collected data as following:

Static Light Scattering results were fitted with a Berry plot where  $\sqrt{I(q)} = \sqrt{I(0)} \left(1 - \frac{q^2 R_G^2}{6}\right)$  [3,4].

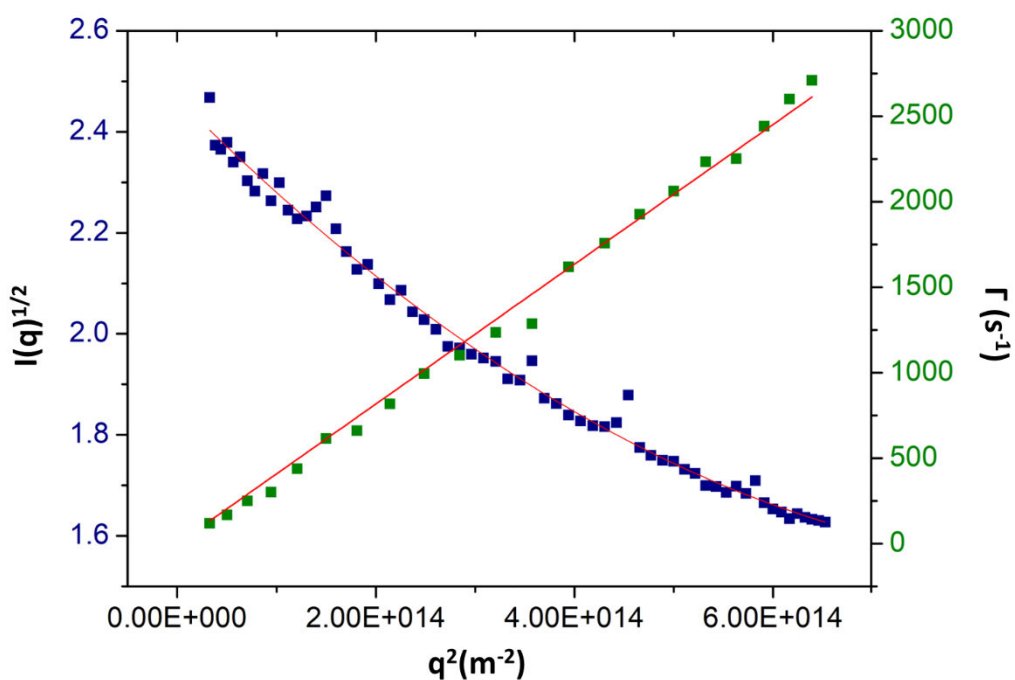
Equation of second order was used to fit the non-linear behavior of the data that might be due to polydispersity. In this case,  $\sqrt{I(x)} = A + Bx + Cx^2$  with  $x = q^2$ .

The radius of gyration  $R_G$  can be isolated using the following relation:  $R_G = \sqrt{\frac{-6B}{A}}$ .

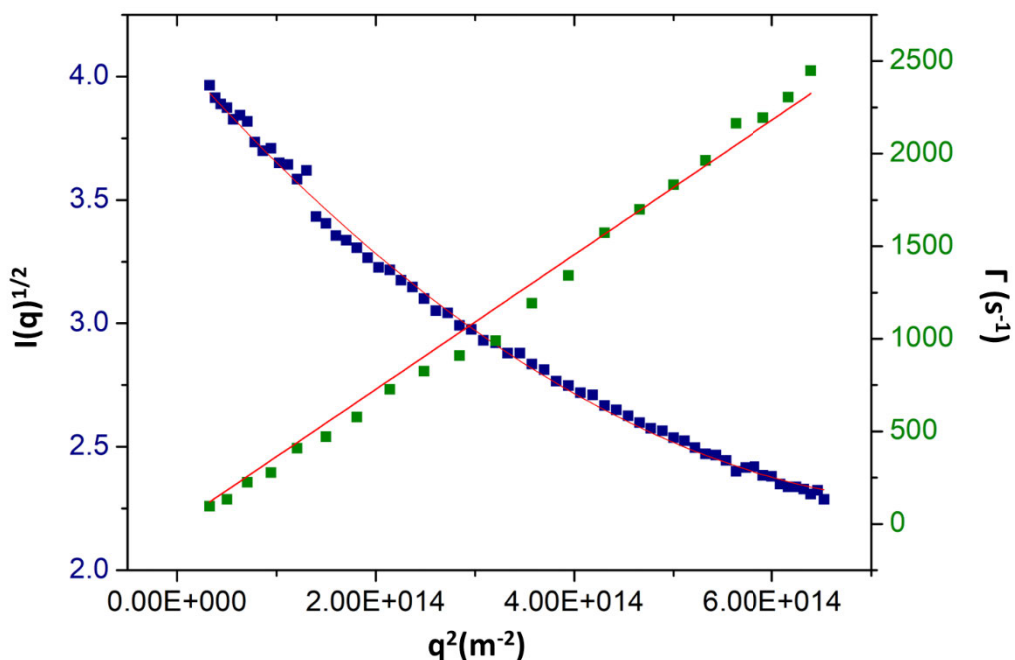
Dynamic light scattering was plotted as  $\Gamma = Dq^2$  according to Fick's law of diffusion where  $D$  ( $\text{m}^2 \cdot \text{s}^{-1}$ ) is the particles diffusion coefficient connected to  $R_H$  by the Stokes-Einstein relation:  $R_H = \frac{k_b T}{6\pi\eta D}$ , with  $k_b$  the Boltzmann constant,  $T$  the temperature (K) and  $\eta$  the solvent viscosity (cP).

Figure S2 to S11 shows SLD and DLS measurements for PEG-*b*-PTMC self-assembled nanoparticles.





**Figure S4** : SLS (blue) and DLS (green) measurements from MALS of a nanoparticles suspension obtained from microfluidic assisted self-assembly of PEG-*b*-PTMC copolymer in a micromixer chip. The final copolymer concentration is 1 mg.mL<sup>-1</sup> and total flow rate is 1000 μL.min<sup>-1</sup>. Linear and non-linear trends are represented by red lines. SLS trend:  $\sqrt{I(x)} = 2.47 - 1.97E-15 x + 1.05E-30 x^2$  ;  $R^2 = 0.9907$ . DLS trend :  $\Gamma(x) = 4.07E-12 x$  ;  $R^2 = 0.9982$ .



**Figure S5** : SLS (blue) and DLS (green) measurements from MALS of a nanoparticles suspension obtained from microfluidic assisted self-assembly of PEG-*b*-PTMC copolymer in a micromixer chip. The final copolymer concentration is 2 mg.mL<sup>-1</sup> and the total flow rate is 1000 μL.min<sup>-1</sup>. Linear and non-linear trends are represented by red lines.. SLS trend :  $\sqrt{I(x)} = 4.079 - 4.55E-15 x + 2.86E-30 x^2$  ;  $R^2 = 0.9968$ . DLS trend :  $\Gamma(x) = 3.64E-12 x$  ;  $R^2 = 0.9965$ .

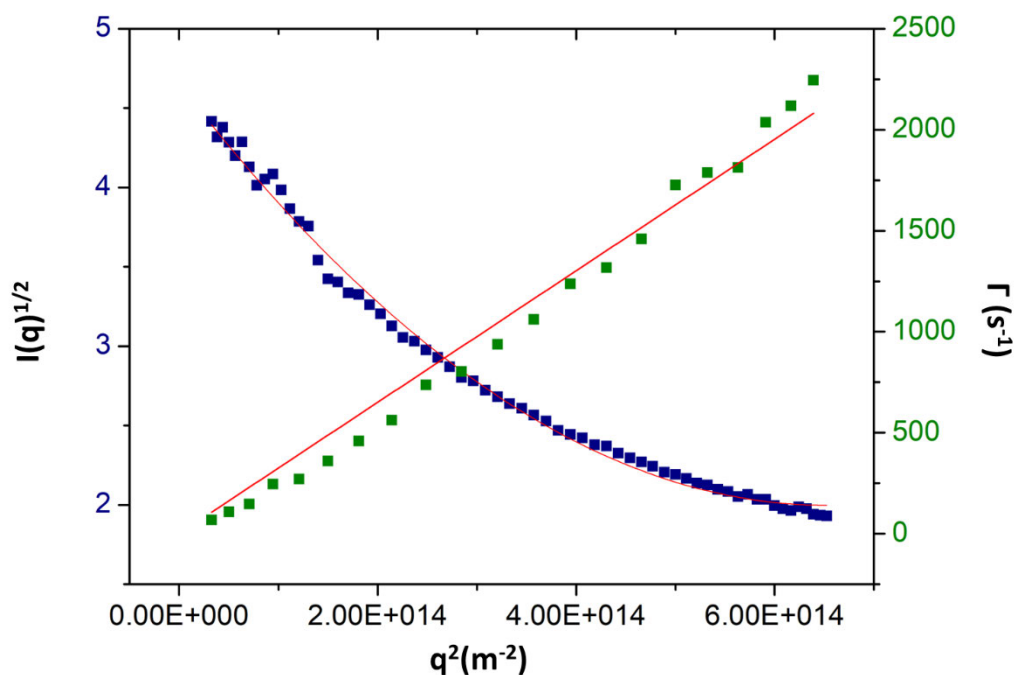


**Figure S6** : SLS (blue) and DLS (green) measurements from MALS of a nanoparticles suspension obtained from microfluidic assisted self-assembly of PEG-*b*-PTMC copolymer in a micromixer chip. The final copolymer concentration is 3 mg.mL<sup>-1</sup> and the total flow rate is 1000 μL.min<sup>-1</sup>. Linear and non-linear trends are represented by red lines. SLS trend :  $\sqrt{I(x)} = 4.65 - 8.13E-15 x + 6.61E-30 x^2$  ;  $R^2 = 0.9949$ . DLS trend :  $\Gamma(x) = 3.26E-12 x$  ;  $R^2 = 0.9935$ .

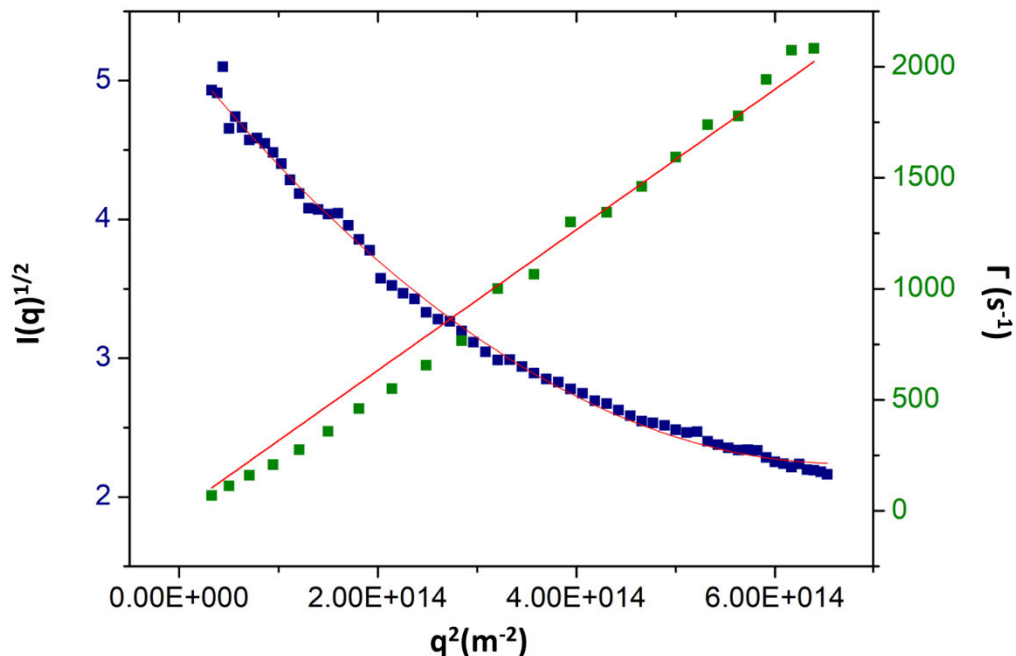


**Figure S7** : SLS (blue) and DLS (green) measurements from MALS of a nanoparticles suspension obtained from microfluidic assisted self-assembly of PEG-*b*-PTMC copolymer in a micromixer chip. The final copolymer concentration is 4 mg.mL<sup>-1</sup> and the total flow rate is 1000 μL.min<sup>-1</sup>. Linear and non-linear trends are represented by red lines. SLS trend :  $\sqrt{I(x)} = 5.21 - 8.86E-15 x + 6.61E-30 x^2$  ;  $R^2 = 0.9952$ . DLS trend :  $\Gamma(x) = 3.16E-12 x$  ;  $R^2 = 0.9952$ .

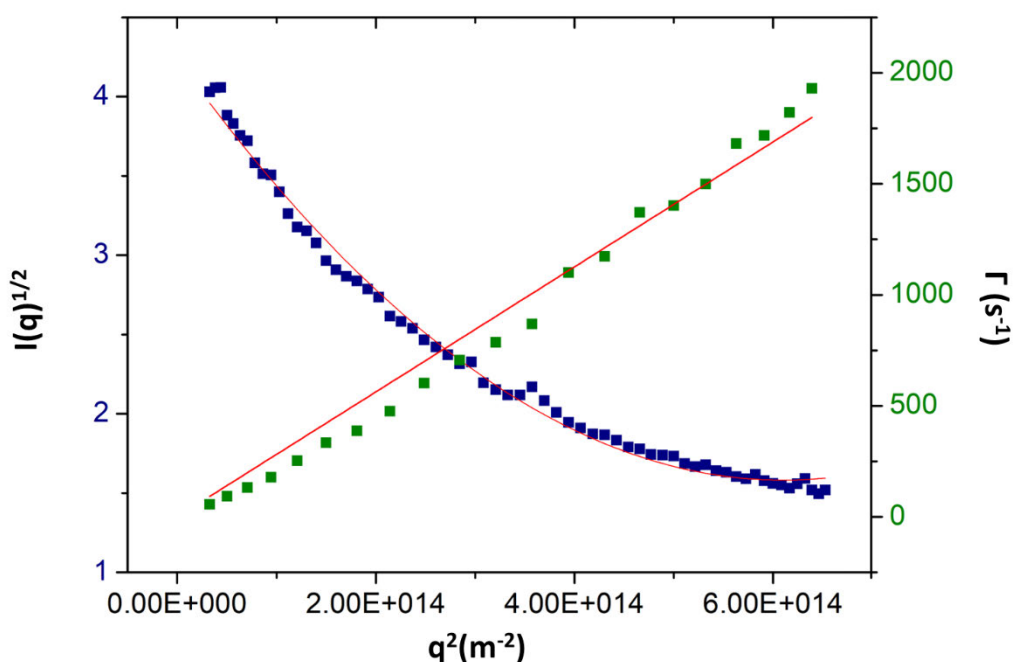


**Figure S8** : SLS (blue) and DLS (green) measurements from MALS of a nanoparticles suspension obtained from microfluidic assisted self-assembly of PEG-*b*-PTMC copolymer in a micromixer chip. The final copolymer concentration is 5 mg.mL<sup>-1</sup> and the total flow rate is 1000  $\mu$ L.min<sup>-1</sup>. Linear and non-linear trends are represented by red lines. SLS trend :  $\sqrt{I(x)} = 4.24 - 8.70E-15 x + 7.13E-30 x^2$  ;  $R^2 = 0.9933$ . DLS trend :  $\Gamma(x) = 2.82E-12 x$  ;  $R^2 = 0.9933$ .

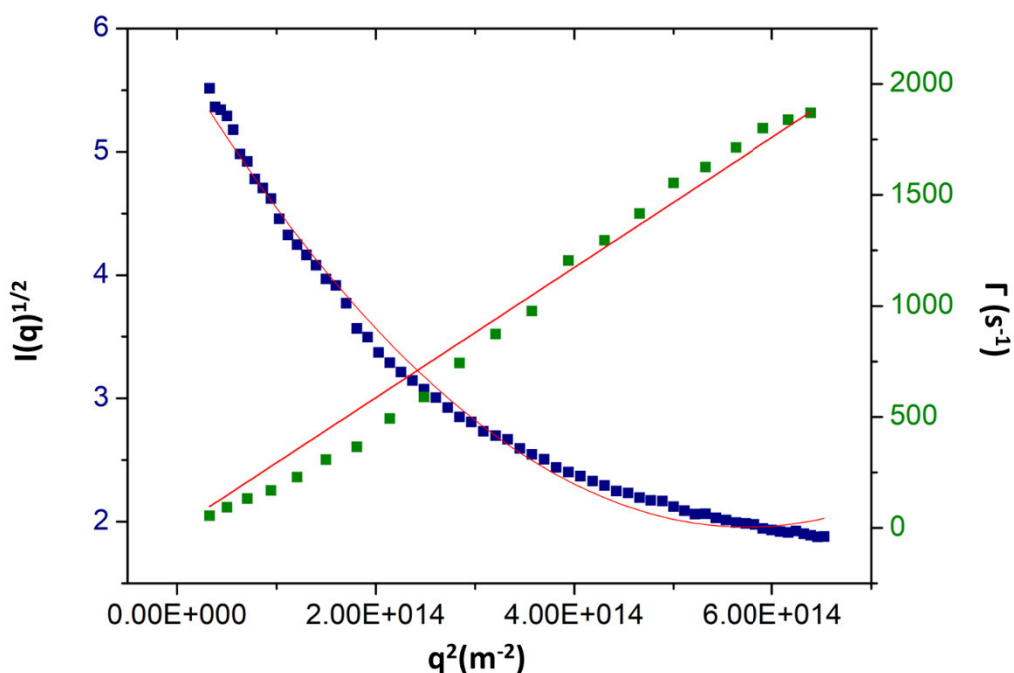


**Figure S9** : SLS (blue) and DLS (green) measurements from MALS of a nanoparticles suspension obtained from microfluidic assisted self-assembly of PEG-*b*-PTMC copolymer in a micromixer chip. The final copolymer concentration is 6 mg.mL<sup>-1</sup> and the total flow rate is 1000  $\mu$ L.min<sup>-1</sup>. Linear and non-linear trends are represented by red lines. SLS trend :  $\sqrt{I(x)} = 5.75 - 1.32E-14 x + 1.15E-29 x^2$  ;  $R^2 = 0.9930$ . DLS trend :  $\Gamma(x) = 2.93E-12 x$  ;  $R^2 = 0.9934$ .

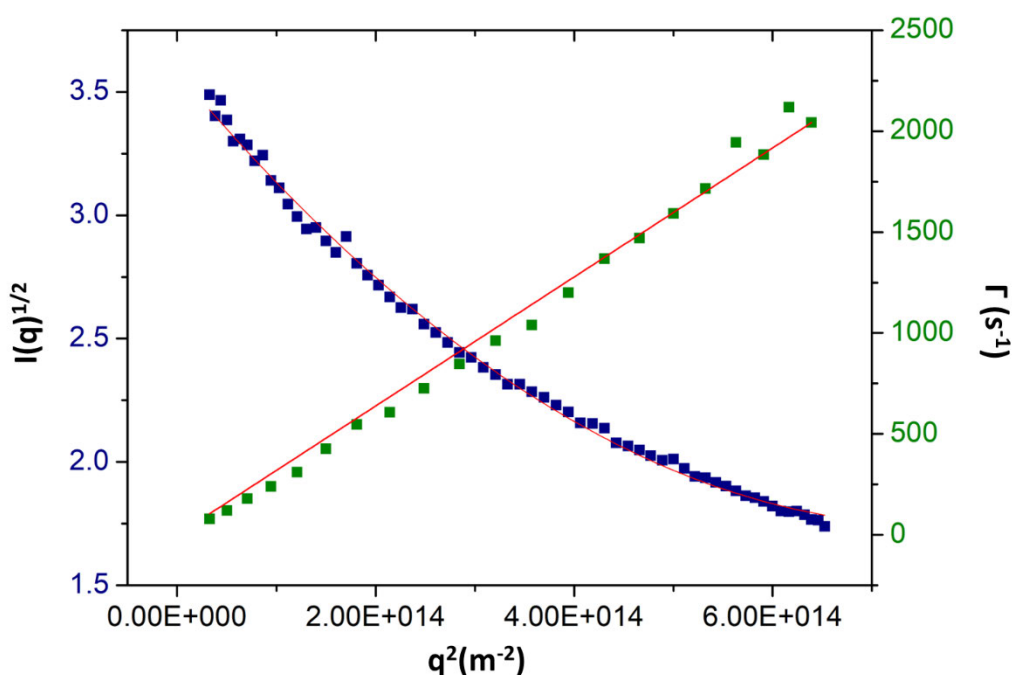


**Figure S10** : SLS (blue) and DLS (green) measurements from MALS of a nanoparticles suspension obtained from microfluidic assisted self-assembly of PEG-*b*-PTMC copolymer in a micromixer chip. The final copolymer concentration is 2 mg.mL<sup>-1</sup> and the total flow rate is 100 μL.min<sup>-1</sup>. Linear and non-linear trends are represented by red lines. SLS trend :  $\sqrt{I(x)} = 3.58 - 4.79E-15 x + 3.13E-30 x^2$  ; R<sup>2</sup> = 0.9969. DLS trend :  $\Gamma(x) = 3.19E-12 x$  ; R<sup>2</sup> = 0.9968.

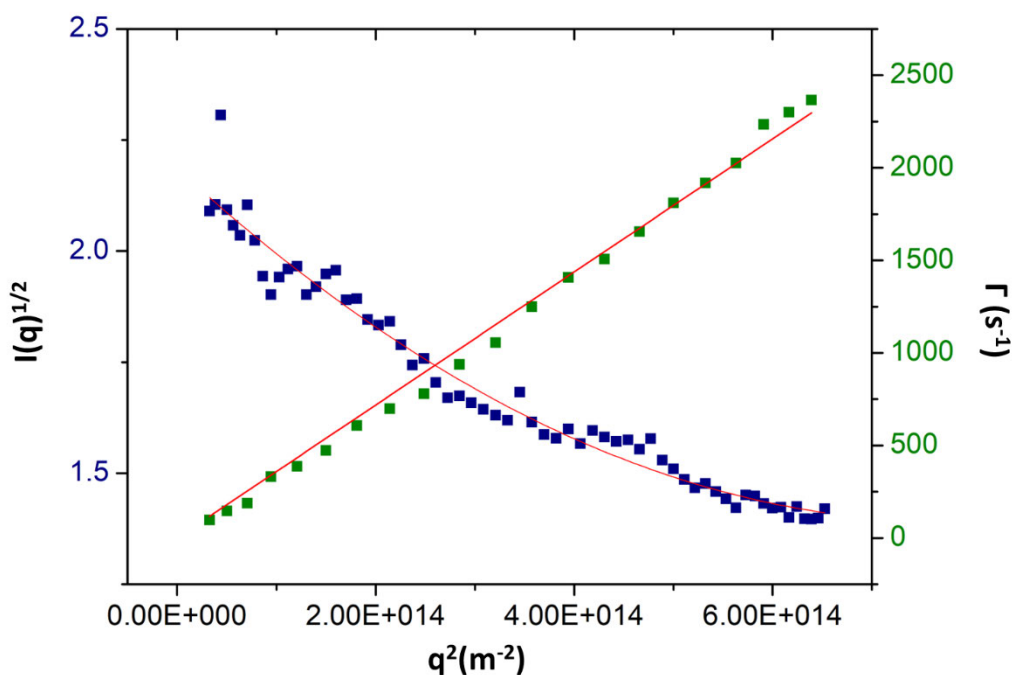


**Figure S11** : SLS (blue) and DLS (green) measurements from MALS of a nanoparticles suspension obtained from microfluidic assisted self-assembly of PEG-*b*-PTMC copolymer in a micromixer chip. Final copolymer concentration is 2 mg.mL<sup>-1</sup> and total flow rate is 200 μL.min<sup>-1</sup>. Linear and non-linear trends are represented by red lines. SLS trend :  $\sqrt{I(x)} = 2.19 - 2.05E-15 x + 1.32E-30 x^2$  ; R<sup>2</sup> = 0.9677. DLS trend :  $\Gamma(x) = 3.59E-12 x$  ; R<sup>2</sup> = 0.9980.

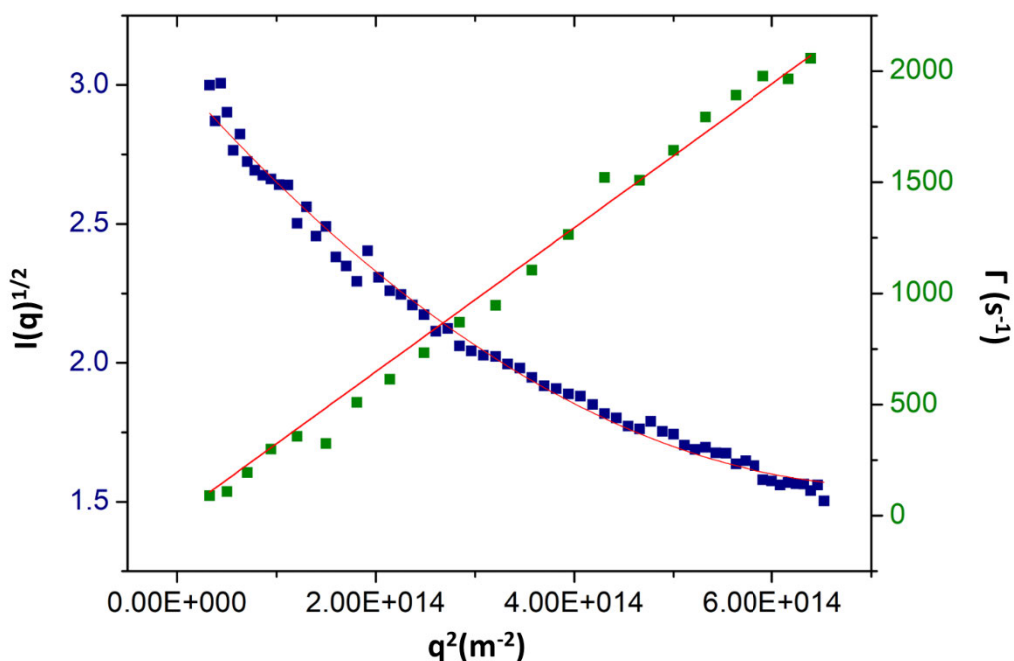


**Figure S12** : SLS (blue) and DLS (green) measurements from MALS of a nanoparticles suspension obtained from microfluidic assisted self-assembly of PEG-*b*-PTMC copolymer in a micromixer chip. The final copolymer concentration is 2 mg.mL<sup>-1</sup> and the total flow rate is 500 μL.min<sup>-1</sup>. Linear and non-linear trends are represented by red lines. SLS trend :  $\sqrt{I(x)} = 3.03 - 4.06E-15 x + 2.79E-30 x^2$  ; R<sup>2</sup> = 0.9906. DLS tend :  $\Gamma(x) = 3.24E-12 x$  ; R<sup>2</sup> = 0.9969.

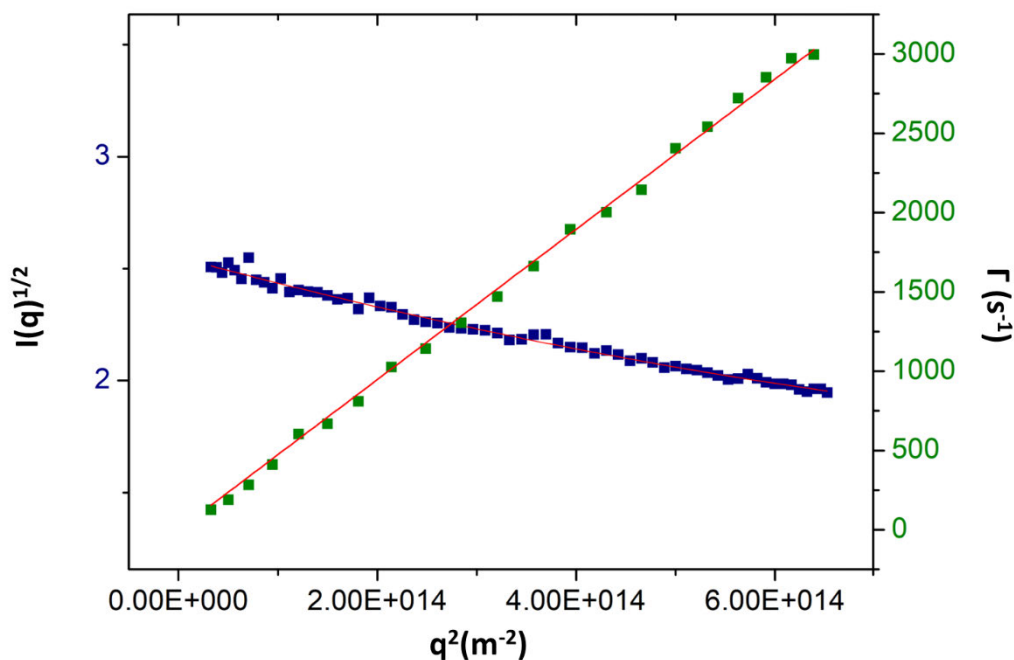


**Figure S13** : SLS (blue) and DLS (green) measurements from MALS of a nanoparticles suspension obtained from microfluidic assisted self-assembly of PEG-*b*-PTMC copolymer in an Herringbone chip. The final copolymer concentration 2 mg.mL<sup>-1</sup> and the total flow rate is 1000 μL.min<sup>-1</sup>. Linear and non-linear trends are represented by red lines. SLS trend :  $\sqrt{I(x)} = 2.55 - 1.19E-15 x + 4.25E-31 x^2$  ; R<sup>2</sup> = 0.9900. DLS trend :  $\Gamma(x) = 4.74E-12 x$  ; R<sup>2</sup> = 0.9994.



**Table S1** : Summary of results from MALS of nanoparticle solutions obtained from microfluidic assisted self-assembly of PEG-*b*-PTMC. Hydrodynamic radius  $R_H$  is obtained from DLS measurement and radius of gyration  $R_G$  is obtained from SLS measurement as previously described.

Microfluidic chip	Copolymer initial concentration (mg.mL <sup>-1</sup> )	Total Flow rate (μL.min <sup>-1</sup> )	$R_G$ (nm) deducted from SLS measurements	$R_H$ (nm) deducted from DLS measurements
Herringbone	10	1000	58	52
Micromixer	10	1000	82	67
	10	500	90	76
	10	200	75	68
	10	100	90	77
	1	1000	33	35
	5	1000	72	60
	10	1000	82	67
	15	1000	102	75
	20	1000	101	76
	25	1000	111	87
	30	1000	117	84

## References

- [1] Lebleu C, Rodrigues L, Guigner J-M, Brûlet A, Garanger E, Lecommandoux S. Self-Assembly of PEG-*b*-PTMC Copolymers: Micelles and Polymersomes Size Control. *Langmuir* 2019;35:13364–74. <https://doi.org/10.1021/acs.langmuir.9b02264>.
- [2] Thiermann R, Mueller W, Montesinos-Castellanos A, Metzke D, Löb P, Hessel V, et al. Size controlled polymersomes by continuous self-assembly in micromixers. *Polymer* 2012;53:2205–10. <https://doi.org/10.1016/j.polymer.2012.03.058>.
- [3] Podzimek S. Light Scattering, Size Exclusion Chromatography and Asymmetric Flow Field Flow Fractionation: Powerful Tools for the Characterization of Polymers, Proteins and Nanoparticles. John Wiley & Sons; 2011.
- [4] Buchholz BA, Barron AE. The use of light scattering for precise characterization of polymers for DNA sequencing by capillary electrophoresis. *Electrophoresis* 2001;22:4118–28. [https://doi.org/10.1002/1522-2683\(200111\)22:19<4118::AID-ELPS4118>3.0.CO;2-Q](https://doi.org/10.1002/1522-2683(200111)22:19<4118::AID-ELPS4118>3.0.CO;2-Q).